Exciton Dynamics in Phthalocyanine Molecular Crystals

Rocco P. Fornari, Juan Aragó,* Alessandro Troisi*

Department of Chemistry and Centre for Scientific Computing, University of Warwick, Coventry CV4 7AL, UK

ABSTRACT

In this paper, the exciton transport properties of an octa(butyl)-substituted metal-free phthalocyanine (H_2-OBPc) molecular crystal have been explored by means of a combined computational (molecular dynamics and electronic structure calculations) and theoretical (model Hamiltonian) approximation. The excitonic couplings in phthalocyanines, where multiple quasi-degenerate excited states are present in the isolated chromophore, are computed with a multistate diabatization scheme which is able to capture both short- and long-range excitonic coupling effects. Thermal motions in phthalocyanine molecular crystals at room temperature cause substantial fluctuation of the excitonic couplings between neighboring molecules (dynamic disorder). The average values of the excitonic couplings are found to be not much smaller than the reorganization energy for the excitation energy transfer and the commonly assumed incoherent regime for this class of materials cannot be invoked. A simple but realistic model Hamiltonian is proposed to study the exciton dynamics in phthalocyanine molecular crystals or aggregates beyond the incoherent regime.

INTRODUCTION

Efficient exciton diffusion in molecular materials or aggregates over long distances is crucial for the performance of photosynthetic light-harvesting systems and photovoltaic applications.[1–4] Two limiting transport regimes (coherent and incoherent) are commonly invoked to describe the exciton diffusion in molecular materials or aggregates.[5] In the coherent regime, the exciton wavefunction is delocalized over several molecular units or, in some cases, over the whole molecular aggregate, whereas in the opposite (incoherent) regime, the exciton wavefunction is completely localized on a molecular unit. Although coherent transport would be highly desirable in terms of efficiency, exciton diffusion in most molecular materials used for optoelectronic applications takes place via a series of hopping events between neighboring molecules, with exciton diffusion lengths that rarely exceed 10 nm.[4] Recent studies, however, have shown that an efficient singlet exciton migration can occur in highly ordered supramolecular materials.[6–8] In particular, Sung et al. have shown by ultrafast transient fluorescence spectroscopy that in helical π-stacks of perylene bisimides delocalized excitons are initially formed and move coherently along the chain in tens of femtoseconds prior to the excimer formation.[6] Haedler et al. have demonstrated that one-dimensional self-assembled nanofibers, based on carbonyl-bridged triarylamine building blocks, are able to efficiently transport singlet excitons over more than 4 μm at room temperature by means of a predominantly coherent mechanism.[7] Heechul et al. have obtained a tunable light-harvesting material, based on a self-assembled chromophore network controlled by a genetically-engineered virus template, which has exhibited enhanced exciton transport via a partially coherent regime.[8] These recent examples clearly highlight the growing interest for obtaining controllable molecular materials for potential nanophotonic and quantum information applications where excitons move beyond the incoherent transport regime. In this sense, it would be

useful to consider model systems for studying partially coherent exciton propagation with a good level of detail.

Phthalocyanine (Pc) derivatives are promising candidates as organic semiconductors for artificial photosynthesis and optoelectronic applications.[9–12] Inspired by their photosynthetic homologous (e.g., bacteriochlorophyll chromophores), different representative examples of self-assembled molecular materials based on Pc building blocks have been synthesized to investigate their exciton transport properties.[13] In contrast to the field of photosynthesis,[2,14,15] in the field of organic electronics a hopping (incoherent) mechanism is generally assumed when the exciton/charge dynamics in Pc-based self-assembled materials is investigated.[4,16,17] However, this assumption is not completely justified in this class of Pc systems since they may present quite large excitonic couplings (20−100 meV) and small exciton-phonon couplings (reorganization energies can be as small as 37 meV).[16,18] A few examples in related self-assembled systems (porphyrins) have shown that exciton diffusion can efficiently occur by means of a coherent mechanism.[19]

Recently, an octa(butyl)-substituted metal-free phthalocyanine, H_2-OBPc (1,4,8,11,15,18,22,25-octabutoxy-29*H*,31*H*-phthalocyanine, see Figure 1a) has been synthesized and exhibited good crystallinity properties (1D π-stacked arrangements, see Figure 1b) in thin films.[20,21] The high degree of crystallinity of the solution-processed thin films allowed Rawat et al. to investigate the correlation between long-range order and the nature of the lowest exciton states of the aggregate.[21] The H_2-OBPc compound is therefore an excellent molecular crystal model to study exciton diffusion at room temperature in the absence of amorphous phase (static) disorder and grain boundaries. The only source of disorder would stem from the intrinsically thermal nuclear motions

(dynamic disorder), which needs to be taken into account for a proper description of the exciton transport.[22,23]

Regardless of the exciton diffusion mechanism invoked, the transport of molecular excitons is mainly governed by the excitonic coupling (J) between the excited states localized on the molecular units (Frenkel excited states).[5,24] In Pc systems, the two lowest-energy singlet excited states (commonly known as Q-bands[25]) are almost degenerate in energy and, thus, both excited states may participate in the exciton transport of Pc molecular crystals or aggregates. Diabatization approximations are particularly suited for evaluating excitonic couplings between several excited states.[26–29] Recently, some of us have developed a diabatization scheme to compute excitonic couplings between molecular crystal pairs beyond the two-level approximation.[30] The great advantage of diabatization schemes is that they can deal with the short-range (exchange and overlap) and long-range (Coulombic) contributions of the excitonic couplings on equal footing. Although the Coulombic coupling is often the only term considered to study exciton transport in molecular aggregates,[31] in organic molecular aggregates or crystals (also in Pc molecular crystals and aggregates), short intermolecular distances in the 3.5–5.5 Å range can be commonly found and, thus, short-range excitonic coupling contributions might become relevant.[32,33] Furthermore, short-range excitonic interactions, unlike the long-range counterpart, are extremely sensitive to the mutual position of the interacting molecular units and, therefore, can undergo significant fluctuations owing to the thermal molecular motions.[22] The thermal fluctuation of the excitonic couplings (also known as non-local exciton-phonon coupling) must be taken into account for a quantitative description of the exciton diffusion and other related phenomena in molecular crystals.[23,34]

In this paper, we investigate the exciton transport of the H_2-OBPc molecular crystal (Figure 1) by means of a combined computational (molecular dynamics and electronic structure calculations) and theoretical (model Hamiltonian) approximation. First, we evaluate the total excitonic couplings between all the relevant excited states in the molecular crystal dimers belonging to the 1D stack (Figure 1c) by a multistate diabatization scheme and analyze the behavior of the couplings as a function of the intermolecular distance. Second, the thermal fluctuation of the excitonic couplings in the most relevant molecular crystal dimers is calculated. Third, the plausible exciton transport regimes are discussed using the computed parameters for this material to determine the most appropriate regime in this case. The exciton dynamics are finally studied with an appropriate theoretical approximation where the thermal excitonic coupling fluctuations have been properly taken into account.

METHODS

1. Diabatization Scheme for Excitonic Couplings

Excitonic couplings in molecular dimers are computed by means of a recently developed diabatization scheme capable of dealing with multiple excited states.[30] Similar in spirit to other diabatization approximations,[35–40] this diabatization process makes use of a molecular property (in this case the atomic transition charges[41]) to find the best adiabatic-to-diabatic orthogonal transformation matrix (**C**) relating the computed adiabatic Hamiltonian ($\mathbf{H}^{A}$) to the diabatic one ($\mathbf{H}^{D}$) as $\mathbf{H}^{D} = \mathbf{C}^{T}\mathbf{H}^{A}\mathbf{C}$, where $\mathbf{C}^{T}$ is the transpose matrix of **C**. The diagonal and off-diagonal elements of $\mathbf{H}^{D}$ correspond to the diabatic energies and the excitonic couplings (J_{ij}), respectively.

Diabatization approaches to evaluate excitonic couplings in molecular crystal pairs are prefered because both the short-range and the long-range effects (all electronic

interactions) can be taken into account. Short-range excitonic coupling contributions are present in molecular crystals or aggregates[32,33] and also are mainly responsible for the fluctuation of the excitonic coupling due to the thermal nuclear motions.[22] It should be stressed that, in the employed diabatization scheme, the phase of the wavefunction can be easily kept constant by controlling the sign of the atomic transition charges (the property used to diabatize). This is of great relevance, for instance, to calculate the time evolution of exciton couplings along a molecular dynamics simulations as we will do here.

2. Molecular Dynamics Simulation of the Crystal

To model the thermal nuclear motions in the H_2-OBPc molecular crystal, we have performed a molecular dynamics (MD) simulation. A 3 × 3 × 3 supercell of the H_2-OBPc crystal was built by replicating the unit cell along each crystallographic axis. The standard MM3 force field was modified to reproduce the equilibrium structure of H_2-OBPc computed at the LC-ωPBE/6-31G** level, i.e., to be consistent with the electronic structure calculations that are based on these classical simulations (see the Supporting Information for further details). The MD simulation was run at room temperature (300 K) and constant volume using the Tinker package.[42]

3. Quantum Chemical Calculations

To estimate the reorganization energy (λ) for an excitation energy transfer reaction (see the Supporting Information),[23] optimizations of the ground state and first two excited states of the H_2-OBPc monomer were calculated in the framework of the density functional theory (DFT) and time-dependent density functional theory (TDDFT) by using the long-range corrected LC-ωPBE[43] density functional and the 6-31G** basis set.[44] A ω value of 0.3 a_0^{-1} for the long-range corrected functional has been employed because it has

been found to be an optimal value that provide a root mean square error (RMSE) of 0.3 eV for both localized and charge-transfer excitations in a large set of medium-sized molecules.[45] On the resulting ground-state optimized geometry, harmonic vibrational frequencies were also computed to obtain the Huang-Rhys factors as carefully explained in ref. 46.

250 snapshots from the MD simulation were taken at time intervals of 50 fs. A cluster of three H_2-OBPc molecules was extracted from each snapshot to compute the excitonic couplings for dimers A and B (Figure 1). To be able to calculate the excitation energies and the atomic transition charges (the molecular properties needed for the diabatization) for 500 dimers (180 atoms per dimer), the calculations were performed at the TDDFT/LC-ωPBE/3-21G* level. This approximation was validated by comparing the excitonic couplings obtained at this level of theory with a small subset of couplings computed at the TDDFT/LC-ωPBE/6-31G** level (see Figure S2). The LC-ωPBE functional has been selected because it should be able to provide an accurate and balanced description of valence and charge-transfer excitations and avoids the typical underestimation of the charge-transfer excitations found in standard hybrid density functionals.[45] It should be noted that in the quantum chemical calculations of both the monomer and the dimer of H_2-OBPc the butoxy chains have been replaced by methoxy groups to alleviate the computational cost since they do not have a significant impact on the electronic structure of H_2-OBPc. It should be also noted that the diabatization scheme does not explicitly make a choice of electromagnetic gauge but inherits the gauge used in the electronic structure calculations, which, as customary, use the Coulomb gauge. All quantum chemical calculations have been performed by using the NWChem 6.6 program package.[47]

RESULTS AND DISCUSSION

1. Excitonic Couplings between Multiple Excited States in H_2-OBPc

The H_2-OBPc crystal presents a pronounced 1D crystal packing along a particular crystalline direction (Figure 1b) with short π-π intermolecular distances in the 3.5–4.5 Å range between nearest neighbors (see ref. 20 for further crystallographic details). Interactions between the 1D columns are relatively small and can be neglected (Figure S3). In the 1D packing, two different molecular pairs (dimers A and B) with the closest intermolecular contacts can be defined (Figure 1c). Both dimers interact through the isoindole groups by means of π-π interactions; specifically, dimer A interacts through the hydrogen-free isoindole-like groups whereas dimer B through the isoindole-like groups. It should be noted that the H_2-OBP molecule at the crystal structure is not planar and, therefore, the position of the central hydrogens can be unambiguously inferred from the geometry of the central cavity (the opposite nitrogen atom pairs connected to H atoms are more distant).

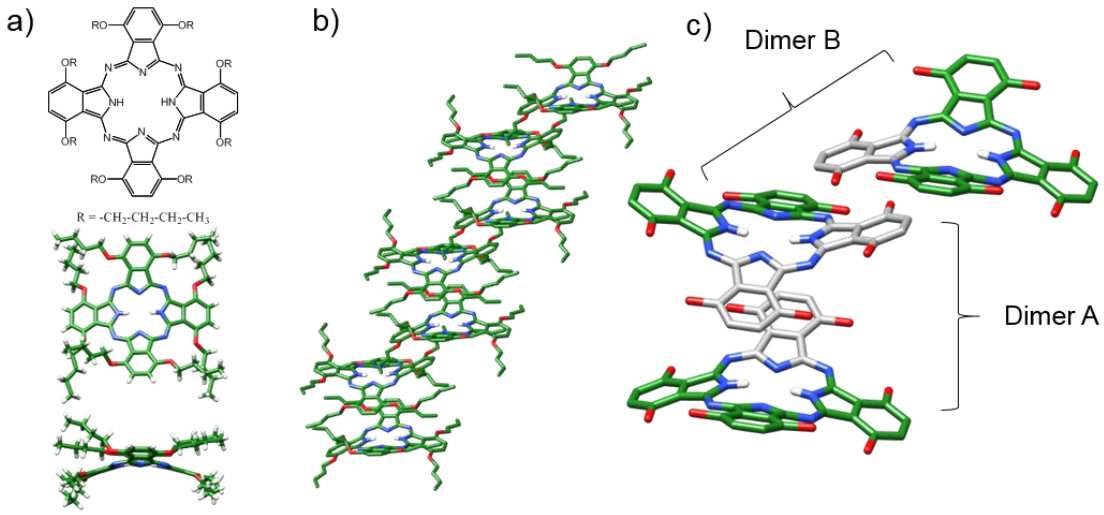

Figure 1. a) Chemical structure and geometry of the H_2-OBPc molecule in the crystal, b) packing of the molecules along the crystalline axis [110][20,21] and c) magnification of the

three central molecules in b to show the structure of the two relevant molecular dimers (A and B) for the exciton transport. The interacting isoindole groups with the shortest intermolecular contacts are depicted in gray, hydrogens (in b and c) and octabutoxy chains (in c) have been omitted for clarity.

The first two excited states S_1 and S_2 of the H_2-OBPc molecule in the crystal geometry were computed at 1.73 and 1.74 eV and can be described as one-electron promotions from the highest occupied molecular orbital (HOMO) to the lowest unoccupied molecular orbitals (LUMO and LUMO+1), see Figure S1. The S_1 and S_2 states present transition dipole moments polarized in almost perpendicular directions with similar oscillator strengths (Figure S1). These computed excited states correspond to the experimental peaks recorded at 1.64 and 1.68 eV in solution (commonly known as the Q_x and Q_y electronic transitions).[21] Higher excited states belonging to the so-called B-band are found to be at least 1.67 eV higher in energy than the S_2 excited state. Therefore, the subspace formed by the first two excited states (Q_x and Q_y) localized on each molecule would be enough to study the exciton dynamics in the H_2-OBPc crystal and the excitonic couplings in dimers A and B would stem mainly from the interactions between these localized Q_x and Q_y states, giving rise to four intermolecular excitonic couplings (J_{xx}, J_{xy}, J_{yx}, and J_{yy}, *vide infra*).

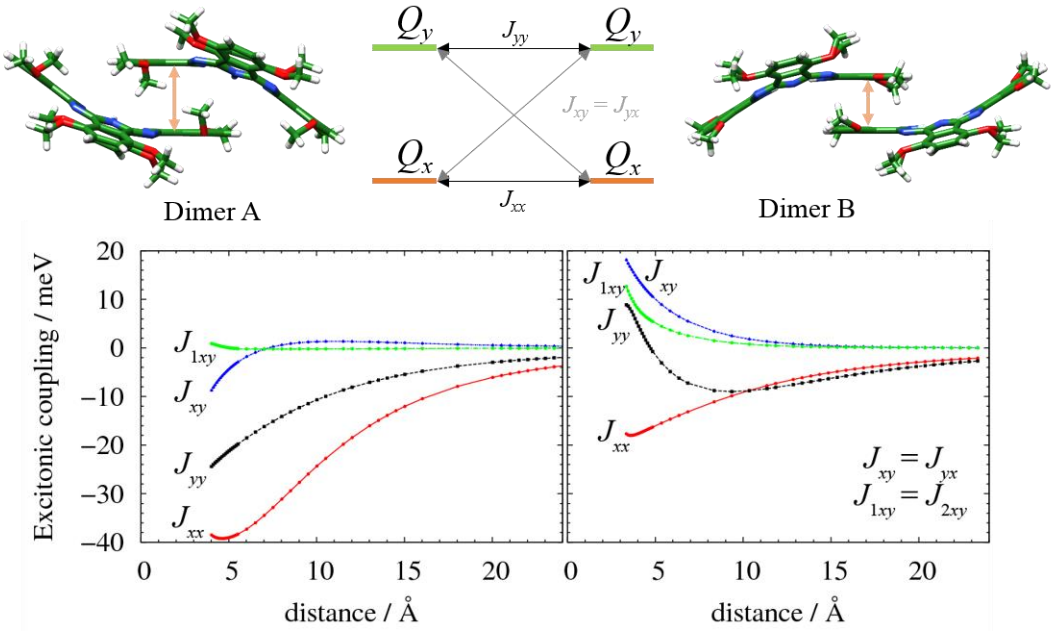

Figure 2. Excitonic couplings as a function of the intermolecular π-π stacking distance between the planes formed by the isoindole rings for dimers A and B at the LC-ωPBE/3-21G* level. The lowest intermolecular contact corresponds to the crystal equilibrium distance.

The total excitonic couplings (short-range and long-range interactions) in dimers A and B have been computed first at the crystal structure equilibrium geometry. For each dimer, a 4 × 4 diabatic Hamiltonian matrix is obtained with six off-diagonal excitonic couplings elements (see diagram in Figure 2 and the Supporting Information). These off-diagonal elements correspond to the intramolecular (J_{1xy} and J_{2xy}) and intermolecular (J_{xx}, J_{xy}, J_{yx}, and J_{yy},) excitonic couplings between the diabatic excited states Q_x and Q_y. The intramolecular J_{1xy} and J_{2xy} excitonic couplings should be in principle close to zero and will be discussed below. The J_{xx}, J_{xy}, J_{yx}, and J_{yy} couplings for dimer A (dimer B) are computed to be −38.51, −8.77, −8.71, and −24.40 meV, respectively (−17.68, 18.12, 18.12, and 8.86 meV, respectively). In general, dimer A presents slightly stronger excitonic couplings than dimer B, especially the J_{xx} coupling.

Figure 2 displays the evolution of all the intermolecular (J_{xx}, J_{xy}, J_{yx}, and J_{yy}) and intramolecular (J_{1xy} and J_{2xy}) excitonic couplings as a function of the intermolecular distance between the planes formed by the isoindole groups. All the excitonic couplings approach to zero with the increase of the intermolecular distance between the monomers. Nevertheless, at long distances (> 20 Å) the largest J_{xx} and J_{yy} couplings in both dimers A and B still present significant values (absolute values in the 5–10 meV range) as a consequence of the long-range Coulombic coupling effects. A further inspection of Figure 2 reveals that the intramolecular J_{1xy} and J_{2xy} excitonic couplings for dimers A and B are not completely negligible at short intermolecular distances, especially for dimer B which presents significant values around 12 meV.

Short-range interactions are also evident from the non-monotonous behavior of some of the excitonic coupling with the intermolecular distance. To analyze this further, we have compared the total intermolecular excitonic couplings with the purely Coulombic excitonic couplings as a function of the intermolecular distance between the planes formed by the isoindole groups (Figure S4). At long intermolecular distances the total excitonic couplings are, as expected, almost identical to the Coulombic couplings computed from the atomic transition charges (ATC) of the two excited states of the isolated molecules (see the Supporting Information). Only at short/intermediate intermolecular distances, the non-Coulombic short-range effects are not negligible. At 4.0 Å for dimer A (i.e., crystal structure), the short-range coupling component, calculated as the difference between the total and Coulombic coupling, is −11.27, −8.54, and −7.92 meV for J_{xx}, J_{xy}, and J_{yy}, respectively. For dimer B, a similar short-range coupling component for the J_{xx}, J_{xy}, and J_{yy} couplings is found (−12.36, 9.36, and 2.24 meV at crystal structure, 3.35 Å). The results highlight the importance of the short-range excitonic coupling component at short intermolecular distances in agreement with other

authors[32,33] and, thus, the necessity of computing the excitonic couplings with proper diabatization schemes able to capture short- and long-range effects on equal footing. Additionally, the short-range interactions are of great relevance since they determine the fluctuation of excitonic couplings owing to thermal nuclear motions.[22]

As mentioned above, the intramolecular excitonic couplings should be close to zero because they come from the interactions between the Q_x and Q_y states located in the same molecule and with almost perpendicular transition dipole moments. However, in a dimer, the excited states localized on the same molecule may be now mixed owing to the presence of the other molecule. To explore this in more detail, we have computed the excitonic couplings between the first two excited states in a model that consists of a dimer of a H_2-OBPc molecule and the interacting isoindole group of the other molecule (Figure S6). The couplings J_{Ixy} for the models at the geometries of dimers A and B are 1.89 and 12.36 meV, respectively, and are in good agreement with the values computed for the whole dimers (0.97 and 12.66 meV). Therefore, these findings clearly show that the non-negligible intramolecular coupling values are not an artifact of the diabatization process but arise as a consequence of the perturbation caused by the adjacent molecule.

2. Thermal Fluctuations of the Excitonic Couplings

Figure 4 displays the time evolution and distributions of the relevant (intermolecular) excitonic couplings (J_{xx}, J_{xy}, J_{yx}, and J_{yy}) for dimers A and B and Table 1 collects the average and standard deviation of each excitonic coupling computed for a total of 250 snapshots separated by 50 fs. All excitonic couplings seem to be normally distributed. The thermally averaged excitonic couplings J_{xx} and J_{yy} for dimer A are found to be −39.25 and −24.29 meV, respectively; i.e., very similar to the couplings computed at the equilibrium crystal structure reported in the previous section, while the average cross-

couplings J_{xy} and J_{yx} are larger (in absolute value) than the crystal values. Unlike dimer A, dimer B presents similar average excitonic couplings around 18 meV for J_{xx} and the cross-couplings, whereas the average of J_{yy} is larger than the crystal value. Both dimers exhibit significant standard deviations (σ_{ii}) of approximately one fifth of the average coupling values, in agreement with the standard deviations found for other molecular crystals.[22,23] In order to identify the vibrations responsible for the excitonic coupling fluctuations, the Fourier transformation of the autocorrelation function $\left\langle \delta J_{ij}(0)\delta J_{ij}(t)\right\rangle$ has been computed, where $\delta J_{ij}(t) = J_{ij}(t) - \left\langle J_{ij}(t)\right\rangle$ is the deviation from the average coupling. Despite the low resolution of the spectral densities shown in Figure S8, the findings seem to suggest that low frequency vibrations below 100 cm^{-1} as well as a vibration just above 300 cm^{-1} are mainly responsible for the modulation of the couplings. These results would be in agreement with higher-resolved spectral densities computed for other molecular crystals in the context of charge and exciton transport where only low-frequency vibrations were identified to be responsible for the modulation of the excitonic couplings.[22,23,48]

Moreover, possible correlations between the excitonic couplings (J_{xx}, J_{xy}, J_{yx}, and J_{yy}) in different dimers have been analyzed (Table S1). The correlation factor, $|cor\left(J_{ij}^{A}, J_{ij}^{B}\right)|$, for all the excitonic couplings is in general computed to be below 0.25, indicating a modest correlation between the excitonic couplings between dimers (see the Supporting Information). The correlation values are similar to those found for charge transfer integrals (electronic couplings) between dimers in the family of oligoacenes.[48]

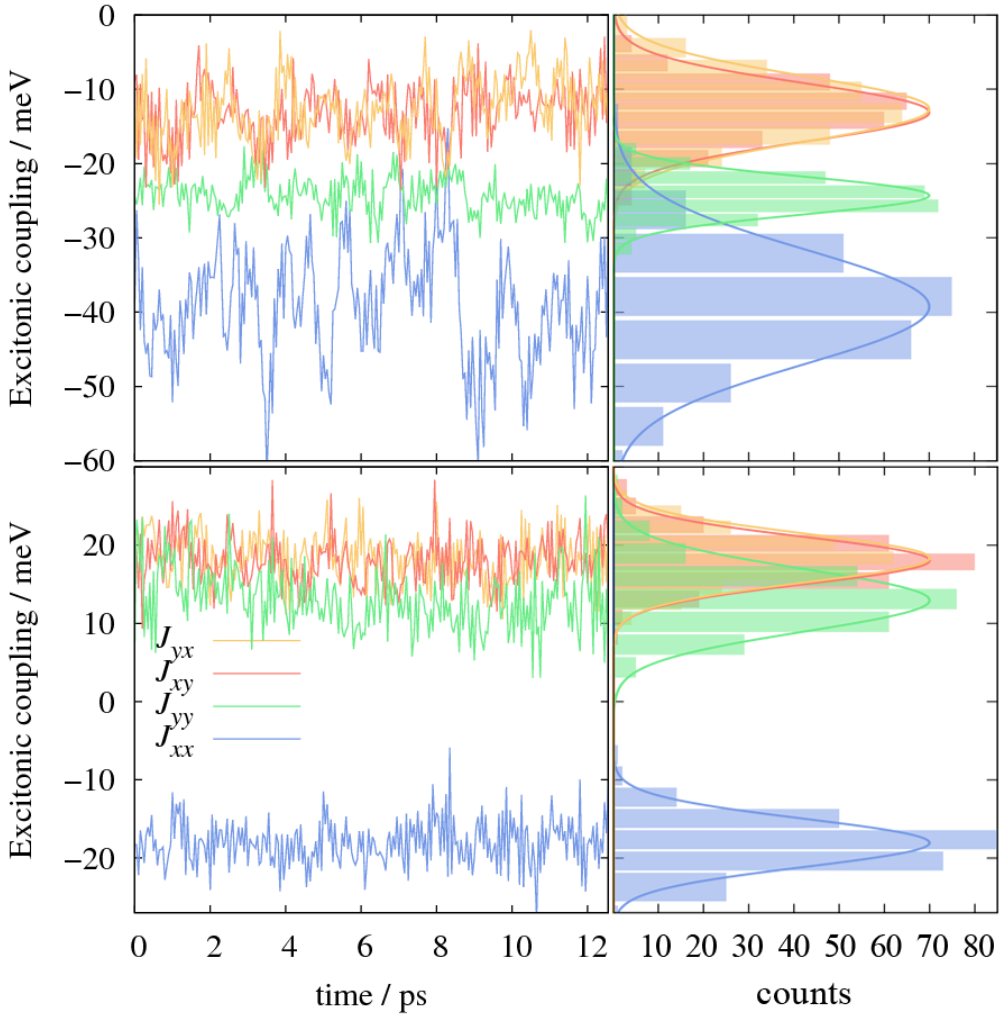

Figure 3. Time evolution (left) and distributions (right) of the excitonic couplings computed at 300 K for the dimers A (top) and B (bottom).

Table 1. Average and Standard Deviations in meV for all the Intermolecular Excitonic Couplings Computed for Dimer A and B.

States	Dimer A		Dimer B	
	$\langle J_{ij} \rangle$	σ_{ij}	$\langle J_{ij} \rangle$	σ_{ij}
xx	−39.25	7.71	−18.07	3.07
xy	−13.11	3.92	18.03	3.01
yx	−12.64	4.40	18.35	3.12
yy	−24.29	2.53	12.94	3.98

3. Local Exciton-Phonon Coupling and Plausible Exciton Transport Regime

In addition to the excitonic coupling between the electronic excited states (discussed above), the coupling between the electronic excited states and the vibrations localized on the molecular moieties (generally known as local exciton-phonon coupling) is also crucial for the exciton transport. In an excitation energy transfer, the local exciton-phonon coupling can be evaluated by means of the reorganization energy (λ). The total reorganization energy λ consists of two contributions that reflect the molecular relaxation energies of one molecule (which is excited) going from the fully relaxed ground state to the electronic excited state and a neighboring molecule (which is de-excited) evolving in the opposite manner (see the Supporting Information).[49]

The total reorganization energy λ for an excitation energy transfer between two H_2-OBPc molecules for the $S_0 \rightarrow S_1$ and $S_1 \rightarrow S_0$ electronic transitions is computed to be 110.89 meV at the LC-ωPBE/6-31G** level. As mentioned above, the reorganization energy stems from two energy relaxation contributions (λ_{S_1} and λ_{S_0}), which can be decomposed into the individual energy contributions of each normal mode by, for example, $\lambda_{S_1} = \sum_k S_k \hbar\omega_k$, where S_k denotes the Huang-Rhys factor for the normal mode *k*. Huang-Rhys factors are computed by projecting the difference between the equilibrium geometries of the two electronic states involved (e.g., S_0 and S_1) on each normal mode computed for the ground state (assuming similar normal modes and frequencies in both electronic states, displaced undistorted harmonic oscillator model, see for instance ref. 46 for further details). Figure 4 (left) displays the individual relaxation energy contribution for each vibration ($S_k \hbar\omega_k$) of the H_2-OBPc molecule and clearly reveals that the relaxation energy is mainly dominated by the contribution of the vibration at 1660 cm^{-1},

which can be mainly described as a collective stretching of the C=N/C=C/C−C bonds of the π-conjugated backbone. The strongest coupling of the high-frequency vibration at 1660 cm^{-1} between S_0 and S_1 is in reasonable agreement with the energy spacing of the vibronic progression (~1500 cm^{-1}) experimentally observed in the absorption spectrum of the metal-free Pc with and without peripheral chains for the Q_x and Q_y bands.[50,51] The similar progression observed for both bands suggest that the same exciton-phonon coupling pattern is expected for the two first electronic transitions ($S_0 \rightarrow S_1$ and $S_0 \rightarrow S_2$). This is confirmed by the analysis of the Huang-Rhys factors computed for the $S_0 \rightarrow S_2$ electronic transition (Figure S11), where the relaxation energy λ_{S_2} is also dominated by the contribution of the vibration at 1660 cm^{-1}. The total λ for the excitation energy transfer involving S_0 and S_2 is calculated to be 158.73 meV. The analysis of the exciton dynamics is significantly simplified if one defines a single effective reaction coordinate with vibrational frequency $\hbar\omega_{eff} = \sum_k S_k \hbar\omega_k \Big/ \sum_k S_k$ with the total associated Huang-Rhys factor $S_{eff} = \sum_k S_k$. The effective vibration frequencies for the relaxation energies λ_{S_1} and λ_{S_2} are calculated to be 1164 and 1192 cm^{-1}, respectively.

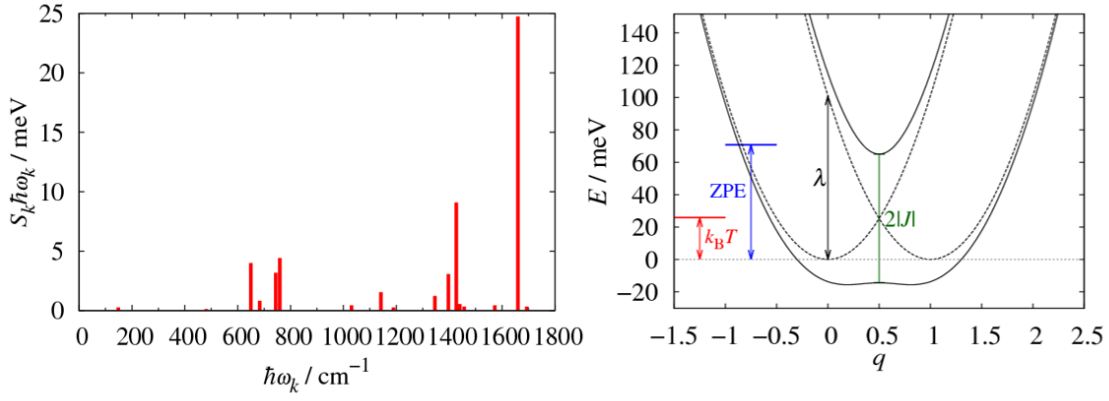

Figure 4. Individual relaxation energy contribution for each normal mode (left) and representation (right) of the diabatic (dotted lines) and adiabatic (solid lines) potential

energy surfaces computed with the average exciton coupling for dimer A ($|\langle J_{xx} \rangle|$) and the total reorganization energy previously computed (λ = 110.89 meV). The thermal energy ($k_B T$) and zero point energy (E_{ZPE}) are also given.

The interplay between the excitonic coupling and the strength of the local exciton-phonon coupling determines the regime for the exciton transport in a molecular crystal or aggregate. When λ is much larger than the (average) excitonic coupling J, the exciton is localized on an individual molecular unit and the exciton transport occurs by means of a sequence of (incoherent) hops with a specific exciton transfer rate. Conversely, when λ is smaller or similar to the excitonic coupling, excitons can be delocalized over several molecules. Evaluating J and λ is therefore a requirement to identify the plausible regimes of exciton transport in a given molecular crystal.

Figure 4 (right) shows the diabatic and adiabatic potential energy surfaces (PES) computed for the excitation energy transfer reaction (D*A → DA*, where D and A stands for donor and acceptor, respectively) along an effective reaction coordinate. With the parameters previously computed for the states S_1 in dimer A ($|\langle J_{xx} \rangle|$ = 39.25 meV and λ = 110.89 meV), the adiabatic PES shows two minima separated by a very small energy barrier (2.37 meV). The thermal energy ($k_B T$ = 25.85 meV) and the zero point energy (E_{ZPE}), estimated as $E_{ZPE} = 1/2\hbar\omega_{eff}$ = 72.16 meV, are also included for comparison purposes. The exciton is therefore delocalized between the two molecular units. It is also interesting to analyze the adiabatic PES computed with the parameters calculated for dimer B ($|\langle J_{xx} \rangle|$ = 18.07 meV and λ = 110.89 meV) in Figure S12. In this particular case, two well-defined minima are found, separated by an energy barrier (12.60 meV) higher than that obtained in dimer A. Nevertheless, it is important to stress that even the thermal

energy k_BT would already be enough to overcome the energy barrier between the two adiabatic minima and the exciton can also be delocalized in both molecular moieties in dimer B. In this context, it seems difficult to be able to assume an incoherent regime for the exciton transport and, therefore, the use of a nonadiabatic transfer rate such as the popular Förster[52] or Marcus[53] rates or even the more sophisticated Marcus–Levi–Jortner (MLJ) rate.[54] For example, by using a general MLJ-type transfer rate recently developed[55] and applied in the context of excitation energy transfer,[23] the exciton transfer rates k_A and k_B between the Q_x excited states for dimer A and B (i.e., only the $\left\langle J_{xx}^2 \right\rangle$ coupling is used) are calculated to be 2.690×10^{13} and 5.649×10^{12} s^{-1}, respectively. These rates are faster than any plausible vibrational relaxation rate[51,56] and are therefore inconsistent with the existence of a rate constant for the process.

Similar values of reorganization energy (λ = 99 meV) and electronic coupling (45 meV) in the context of charge transport for a nonperipheral octahexyl substituted Pc in its crystal and liquid crystal phase have been recently reported.[17] The authors investigated the charge-transport properties of this Pc derivative but invoked directly an incoherent regime for the transport, which seems to be inconsistent with the parameters (λ and the electronic coupling) of this problem. In the next section, we will describe a model able to describe the exciton dynamics in the H_2-OBPc molecular crystal where the incoherent regime does not apply.

4. Exciton Dynamics

The transport in the H_2-OBPc crystal can be assumed to take place mainly within the 1D arrangement with the two alternating dimers A and B (1D transport, Figure 5a). In this situation, a model Hamiltonian able to incorporate the different physical ingredients for

the exciton transport but with a reduced number of degrees of freedom can be derived. This model Hamiltonian is written as:

$$
\begin{aligned}
H = & \sum_{jp}\left(E_{jp} + \sum_{k} g_{jp}^{(k)} q_{j}^{(k)} \right) \left| j_p \right\rangle \left\langle j_p \right| \\
& + \sum_{jpp'}\left(J_{jpp'} + \sum_{k} a_{jpp'}^{(k)} \left(q_{j}^{(k)} - q_{j+1}^{(k)} \right) \right) \left| j_p \right\rangle \left\langle \left(j+1 \right)_{p'} \right| + h.c. \\
& + \sum_{j}\sum_{k}\left(\frac{1}{2} m^{(k)} \left(\dot{q}_{j}^{(k)} \right)^2 + \frac{1}{2} m^{(k)} \left(\omega^{(k)} q_{j}^{(k)} \right)^2 \right)
\end{aligned}
\tag{1}
$$

The index *j* runs over the molecular sites in the 1D assembly (Figure 5a) where the odd and even *j* sites are not equivalent. *p* runs over the excited states of each site. On each molecule, only two singlet excited states (p = 2) and several harmonic nuclear vibration modes (indexed with *k*, with displacement $q_j^{(k)}$, effective mass $m^{(k)}$, and frequency $\omega^{(k)}$) are considered. At equilibrium position ($q_j^{(k)}$ = 0), E_{jp} and $J_{jpp'}$ denote the energy of the *p* singlet excited state at site *j* and the excitonic couplings between the *p* and p' excited states at adjacent molecular sites *j* and *j*+1. The nuclear vibrations in this model Hamiltonian are coupled to the exciton carriers in two different ways. They modify the energy of the *p*th exciton at site *j* according to the linear local exciton-phonon coupling (Holstein coupling[57]) term $g_{jp}^{(k)} q_{j}^{(k)} \left| j_p \right\rangle \left\langle j_p \right|$, where $g_{jp}^{(k)}$ is the local exciton-phonon constant and is related to the reorganization energy. Moreover, the relative displacements between $q_j^{(k)}$ and $q_{j+1}^{(k)}$ modulate the excitonic coupling between the states $\left| j_p \right\rangle$ and $\left| \left(j+1 \right)_{p'} \right\rangle$ through the term $a_{jpp'}^{(k)} \left(q_{j}^{(k)} - q_{j+1}^{(k)} \right)$ where $a_{jpp'}^{(k)}$ quantifies the nonlocal electron-phonon coupling and is related to the magnitude of the thermal fluctuation.

E_{j1} and E_{j2} are set to 0 and 10 meV for all the sites, from the first two excited states computed for the isolated H_2-OBPc molecule in the crystal geometry. The local Holstein exciton-phonon constant $g_{jp}^{(k)}$ is independent from *j* but it is different for the two excited

states per molecule ($g_{jp}^{(k)} = g_{p}^{(k)}$). The analysis of the Huang-Rhys factors computed for H_2-OBPc (Figure 4 and Figure S11) allowed us to define a single effective vibration for each $S_0 \rightarrow S_1$ and $S_0 \rightarrow S_2$ excitation of H_2-OBPc associated with the total reorganization energy (111 and 159 meV, respectively). The frequencies of these two effective modes (k = 1 and k = 2) are set to $\omega^{(1)}$ = 1164 and $\omega^{(2)}$ = 1192 cm^{-1} (144 and 148 meV) and the mass $m^{(1)} = m^{(2)} = 6$ amu (the reduced mass of the C-C/C=C bonds that gives the larger contribution to these modes). Note that the vibration mode k = 1 (k = 2) only modulates the diagonal energy E_{j1} (E_{j2}). The local Holstein exciton-phonon constants are therefore computed as $g_1^{(1)} = \omega^{(1)}\sqrt{m^{(1)}\lambda_{S_0 \rightarrow S_1}}$ = 1821 and $g_2^{(2)} = \omega^{(2)}\sqrt{m^{(2)}\lambda_{S_0 \rightarrow S_2}}$ = 2231 meV $Å^{-1}$. It should be mentioned that the external component of the neighboring molecules (external reorganization energy) on the site fluctuation in molecular crystals is expected to be much smaller than the fluctuation due to intramolecular vibrations and, thus, this environmental effect has not been included.[58,59]

For the off-diagonal elements, the $J_{jpp'}$ couplings when j is an odd site are set to be the average excitonic couplings computed for dimers A whereas the average excitonic couplings computed for dimers B are used when j is an even site (Figure 5a). Similar to the local exciton-phonon coupling, it is also convenient to select an effective mode (or at least a few effective modes) that can capture the overall effect of the low-frequency vibrations on the excitonic coupling in the model Hamiltonian (eq 1). Based on the low-resolved spectral densities shown in Figure S8 and high-resolved spectral densities computed for other molecular crystals in the context of charge and exciton transport,[22,23,48] low-frequency vibrations (10–100 cm^{-1} range) seem to be mainly responsible for the modulation of the excitonic coupling. Correlations between the excitonic couplings fluctuations between dimers A and B were found to be very small (see Table S1). It is

therefore reasonable to assume four independent low-frequency vibrations (k = 3, 4, 5 and 6) as the effective modes coupled strongly to each excitonic coupling. The frequencies of these effective modes can be tentatively estimated from a weighted average of the low-frequency vibrations (< 100 cm^{-1}) of the spectral density (Figure S8) and are found to be very similar ($\omega^{(3)} = \omega^{(4)} = \omega^{(5)} = \omega^{(6)} = 5$ meV). Note that a precise assignment of the frequency of these effective modes is not essential for the exciton transport model. The mass for these effective vibrations is set to be $m^{(3)} = m^{(4)} = m^{(5)} = m^{(6)} =$ 754 amu, which corresponds to the mass of the H_2-OBPc molecule. A specific value for the nonlocal exciton-phonon coupling constant $a_{jpp'}^{(k)}$ can be calculated if it is assumed that only the kth effective mode couples with $J_{jpp'}$. Using the standard deviations previously computed for the excitonic couplings (Table 1), $a_{jpp'}^{(k)}$ can be then computed as $\sigma_{J_{jpp'}} = a_{jpp'}^{(k)} \sqrt{2k_B T \Big/ m^{(k)} \left(\omega^{(k)}\right)^2}$. Table 2 summarizes all the parameters used for the model Hamiltonian (eq 1).

Recently, Schröter and Kühn have analyzed the interplay between local nonadiabatic deactivation effects and Frenkel exciton transfer in molecular perylene bismide aggregates.[60] To do so, they adopted a Frenkel Hamiltonian model in the diabatic representation which was extended to incorporate nonadiabatic couplings between the excitonic bands (adiabatic representation). Although the nonadiabatic effects can be relevant when two excited states are close in energy as it is the case here, our model is able to partially capture these effects because we are allowing for the mixing between the Q_x and Q_y diabatic states (or Q_y and Q_x) localized on each molecular site by the non-zero cross excitonic couplings (J_{xy} and J_{yx}). Note that Schröter and Kühn set these cross couplings to be zero.

As noted in ref. 23, the model proposed is able to include both diagonal (on-site energies) and off-diagonal (excitonic couplings) fluctuations of the electronic Hamiltonian on equal footing, the two terms being respectively the second and fourth term in eq 1. In fact, the model Hamiltonian was constructed to reproduce the amplitude and the timescale of the fluctuations of the excitonic coupling computed from the MD/quantum chemistry procedure. The masses and force constants determine the timescale of the fluctuations and the nonlocal exciton-phonon coupling constants determine their strength.

Table 2. Parameters Used for the H_2-OBPc Crystal Transport Model.

Parameter	Value
N	600
E_{jp}	0 (p = 1) and 10 (p = 2) meV
J_{j11}, J_{j12}, J_{j21}, and J_{j22} (j odd)	−39, −13, −13, and −24 meV
J_{j11}, J_{j12}, J_{j21}, and J_{j22} (j even)	−18, 18, 18, and 13 meV
$g_1^{(1)}$ and $g_2^{(2)}$	1821 and 2231 meV Å^{-1}
$\omega^{(1)}$ and $\omega^{(2)}$	144 and 148 meV
$m^{(1)} = m^{(2)}$	6 amu
$a_{j11}^{(3)}$, $a_{j12}^{(4)}$, $a_{j21}^{(5)}$, and $a_{j22}^{(6)}$ (j odd)	71, 36, 41, and 23 meV Å^{-1}
$a_{j11}^{(3)}$, $a_{j12}^{(4)}$, $a_{j21}^{(5)}$, and $a_{j22}^{(6)}$ (j even)	29, 28, 29, and 37 meV Å^{-1}
$\omega^{(3)} = \omega^{(4)} = \omega^{(5)} = \omega^{(6)}$	5 meV
$m^{(3)} = m^{(4)} = m^{(5)} = m^{(6)}$	754 amu

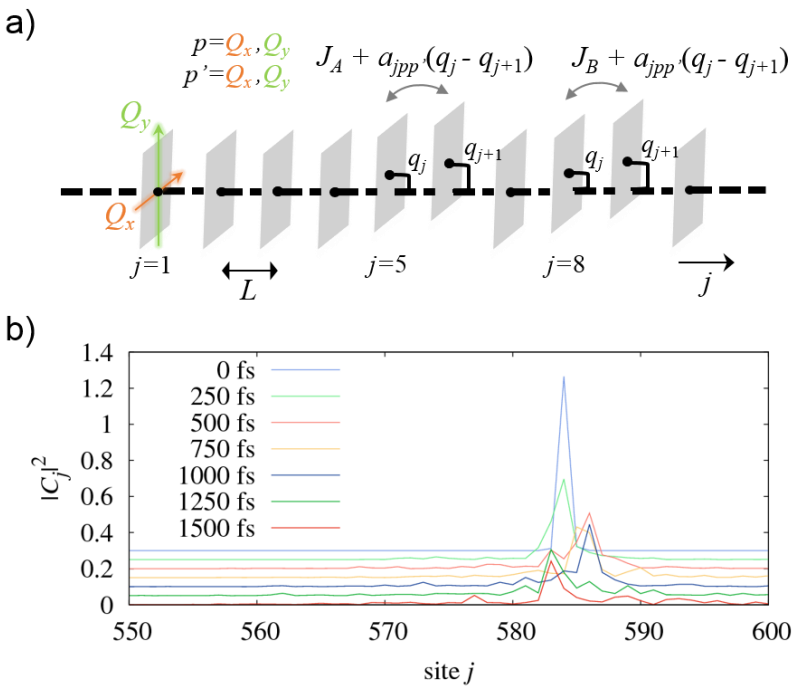

Figure 5. a) Scheme of the 1D model used to describe the exciton transport in the H_2-OBPc molecular crystal and b) time evolution of the exciton wavefunction evaluated from the model Hamiltonian. Populations on each site (vertically off-set for clarity) are reported from t = 0 to t = 1500 fs every 250 fs. Site *j* represents molecules in the model.

The time evolution of the exciton wavefunction can be computed by integrating the model Hamiltonian (eq 1) within an Ehrenfest dynamics scheme, where the nuclear modes are treated classically. Further details of the numerical integration can be found for example in ref. 61. The Ehrenfest scheme has some important limitations extensively discussed in literature;[62] mainly the absence of decoherences and erroneous thermal equilibration at long times. However, it is preferable over surface hopping methods[63] when a quasi continuum of electronic states is present, as in this case.[64,65]

The initial nuclear positions, $q_j^{(k)}(0)$, and velocities, $\dot{q}_j^{(k)}(0)$, for the simulation at temperature *T* were randomly selected from the Boltzmann distribution. The nonlocal exciton-phonon couplings have been chosen so that the distribution of the instantaneous

excitonic coupling at 300 K has the same mean and standard deviation of that computed for the atomistic system at the same temperature (Section 2). In the semiclassical evolution of the system the classical modes oscillates around their equilibrium position with random phases and a thermal distribution of amplitudes modulating the excitonic coupling and reproducing the dynamic disorder observed computationally.

Figure 5b displays the time evolution of the exciton wavefunction. The initial exciton wavefunction, which is selected to be in one of the excitonic eigenstates of the Hamiltonian at the beginning of the simulation (only the lowest-energy wavefunction is shown in Figure 5b), is localized on just a few sites (< 4) at 300 K. The initial localization of the exciton wavefunction is induced by disorder in the diagonal and off-diagonal terms of the electronic Hamiltonian. Nevertheless, the exciton wavefunction spreads as a consequence of the time dependence of the excitonic couplings. The exciton diffusion coefficient along the columns of the H_2-OBPc system can be quantitatively calculated by monitoring

$$R_n^2(t) \equiv \langle \psi_n(t) | r^2 | \psi_n(t) \rangle - \langle \psi_n(t) | r | \psi_n(t) \rangle^2 \qquad (2)$$

which measures the time-dependent spread of the wavefunction. $R_n^2(t)$ is computed from 300 different initial wavefunctions $\psi_n(0)$ (and energies E_n) and averaged (with Boltzmann weight) to give $\langle R^2(t) \rangle$. The initial wavefunctions $\psi_n(0)$ included in the Boltzmann average have been chosen to be those that can be thermally accessible with energies above the lowest-energy eigenstate in the 260 meV range. In this way, different degrees of localization found to be relevant in molecular crystals are taken into account for the estimate of the exciton diffusion coefficient.[66,67] Figure 6 displays the temperature averaged squared displacement $\langle R^2(t) \rangle$ versus time. $\langle R^2(t) \rangle$ increases linearly with time which is indicative of a diffusive behavior. The exciton diffusion coefficient is then

evaluated from the relationship $D = \lim_{t\to\infty} \left\langle R^2(t) \right\rangle / 2t$ (in practice D is evaluated from the longest simulated time of 1.5 ps).[61,68,69] The distance between molecules is set to 8.64 Å (average intermolecular distance between the centers of mass of the H_2-OBPc molecules within the 1D π-stacked arrangement Figure 1b). A value of D = 0.324 cm^2 s^{-1} is obtained for the H_2-OBPc crystal. It should be also noted that the exciton diffusion coefficient computed from the model Hamiltonian (with two electronic states per site) is larger than the exciton diffusion coefficient (D = 0.095 cm^2 s^{-1}) computed from a similar model but with only one electronic state per site (Figure S13). The comparison between both models clearly reveals that the incorporation of the two electronic excited states close in energy (Q_x and Q_y) gives rise to an enhanced exciton transport pathway.

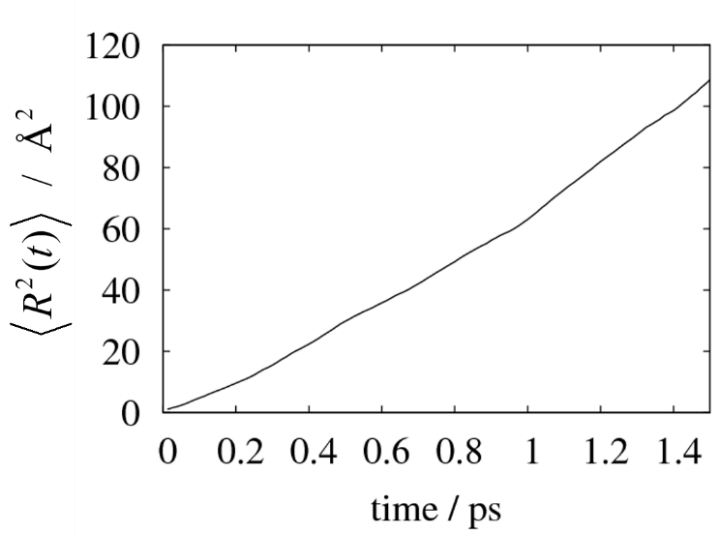

Figure 6. Plot of the temperature averaged square displacement $\left\langle R^2(t) \right\rangle$ (in Å^2) versus time using the parameters of Table 2.

The predicted exciton diffusion coefficient (0.324 cm^2 s^{-1}) is of the same order of magnitude as that reported for a zinc Pc (ZnPc) derivative aggregate (D = 0.43 cm^2 s^{-1}) derived from exciton-exciton annihilation measurements[70] although larger than other

exciton diffusion coefficients of Pc-based amorphous materials.[71] However, the diffusion coefficient of the ZnPc aggregate was estimated by assuming an incoherent regime with an exciton transfer rate of ~1.0×10^{13} s^{-1}, which is close to the limit of validity of a first order rate process in a molecular system. The agreement between the theoretical and experimental exciton diffusion coefficients suggests that the model proposed here is able to correctly describe exciton diffusion, but without assuming an incoherent regime, which would be incompatible with the J and λ parameters of this system (see Section 3). It seems therefore very likely that in Pc aggregates with efficient exciton transport properties at room temperature the exciton diffusion regime (beyond the incoherent) is that limited by the thermal fluctuation of the excitonic couplings (dynamic disorder).

CONCLUSIONS

In this contribution, we have explored the exciton transport properties of an octa(butyl)-substituted metal-free phthalocyanine (H_2-OBPc) molecular crystal by means of a combined computational (molecular dynamics and electronic structure calculations) and theoretical (model Hamiltonian) approximation.

We have shown that the multistate diabatization scheme recently developed is particularly suited for computing the excitonic couplings in molecular dimers of phthalocyanines where multiple quasi-degenerate excited states are present in the isolated chromophore. Short-range excitonic couplings effects, also captured by our computational scheme, are shown to be potentially significant between molecules in close contact.

A significant fluctuation of the excitonic couplings owing to thermal nuclear motions in a phthalocyanine molecular crystal has been found in agreement with other molecular crystals. Low-frequency vibrations have been shown to be responsible for the excitonic

coupling fluctuation. The average values of the excitonic couplings are found to be significant in the 40–18 meV range and not much smaller than the reorganization energy associated with the exciton energy transfer. In this situation, the exciton is delocalized, the commonly assumed incoherent regime for self-assembled phthalocyanine-based molecular aggregates is not valid, and a simple nonadiabatic exciton transfer rate cannot be derived. The results clearly suggest that phthalocyanine-based molecular aggregates may be good candidates for efficient excitation energy transport beyond the Förster (incoherent) mechanism.

A simple but realistic model Hamiltonian able to incorporate multiple excited states per site and fluctuations of the excitonic couplings has been proposed to explore the exciton dynamics of the H_2-OBPc molecular crystal. The fluctuation of the excitonic couplings (dynamic disorder) causes the initial localization of the exciton wavefunction in just a few molecules but also assists in its quick spread. This transport regime, where the off-diagonal fluctuations are of great relevance, is completely different than the transport regimes generally assumed in the context of exciton transport (incoherent) and seems to be adequate for Pc aggregates with efficient exciton transport properties at room temperature. Although the theoretical model proposed can capture the essential effects for the exciton transport, there are some challenging but missing effects (going beyond the 1D model, including quantum vibronic effects and introducing decoherences) that should be incorporated in fully quantitative models.

ASSOCIATED CONTENT

Supporting Information. Force field details, excitation energies computed at LC-ωPBE/6-31G** of the H_2-OBPc monomer, details about the diabatic Hamiltonian and the off-diagonal excitonic couplings, comparison between total and purely Coulombic exciton couplings, the Fourier transformation of the autocorrelation function of the

excitonic couplings, correlation between the excitonic couplings computed for dimers A and B, details about the calculation of the reorganization energy and exciton diffusion coefficient for a simpler model. This material is available free of charge via the Internet at http://pubs.acs.org.

AUTHOR INFORMATION

Corresponding Author

*E-mail: j.arago-march@warwick.ac.uk (J.A). Telephone: +34 963544428

*E-mail: a.troisi@warwick.ac.uk (A.T.). Telephone: +44 (024) 7652 3228

Notes

The authors declare no competing financial interest.

ACKNOWLEDGEMENTS

This work was supported by a Marie Curie Intra European Fellowship within the 7th European Community Framework Programme (FP7-PEOPLE-2012-IEF-329513) and the European Research Council (Grant No. 615834).

REFERENCES

(1) Scholes, G. D.; Mirkovic, T.; Turner, D. B.; Fassioli, F.; Buchleitner, A. Solar Light Harvesting by Energy Transfer: From Ecology to Coherence. *Energy Environ. Sci.* **2012**, *5*, 9374–9393.

(2) Scholes, G. D.; Fleming, G. R.; Olaya-Castro, A.; van Grondelle, R. Lessons from Nature about Solar Light Harvesting. *Nat Chem* **2011**, *3*, 763–774.

(3) Scholes, G. D.; Rumbles, G. Excitons in Nanoscale Systems. *Nat Mater* **2006**, *5*, 683–696.

(4) Menke, S. M.; Holmes, R. J. Exciton Diffusion in Organic Photovoltaic Cells. *Energy Environ. Sci.* **2014**, *7*, 499–512.

(5) May, V.; Kühn, O. *Charge and Energy Transfer Dynamics in Molecular Systems*; Wiley-VCH Verlag GmbH & Co. KGaA: Weinheim, Germany, 2011.

(6) Sung, J.; Kim, P.; Fimmel, B.; Würthner, F.; Kim, D. Direct Observation of Ultrafast Coherent Exciton Dynamics in Helical π-Stacks of Self-Assembled Perylene Bisimides.

Nat. Commun. **2015**, *6*, 8646.

(7) Haedler, A. T.; Kreger, K.; Issac, A.; Wittmann, B.; Kivala, M.; Hammer, N.; Köhler, J.; Schmidt, H.-W.; Hildner, R. Long-Range Energy Transport in Single Supramolecular Nanofibres at Room Temperature. *Nature* **2015**, *523*, 196–199.

(8) Park, H.; Heldman, N.; Rebentrost, P.; Abbondanza, L.; Iagatti, A.; Alessi, A.; Patrizi, B.; Salvalaggio, M.; Bussotti, L.; Mohseni, M.; et al. Enhanced Energy Transport in Genetically Engineered Excitonic Networks. *Nat. Mater.* **2015**, *15*, 211–216.

(9) Bottari, G.; de la Torre, G.; Torres, T. Phthalocyanine-Nanocarbon Ensembles: From Discrete Molecular and Supramolecular Systems to Hybrid Nanomaterials. *Acc. Chem. Res.* **2015**, *48*, 900–910.

(10) Bottari, G.; Trukhina, O.; Ince, M.; Torres, T. Towards Artificial Photosynthesis: Supramolecular, Donor–acceptor, Porphyrin- and Phthalocyanine/carbon Nanostructure Ensembles. *Coord. Chem. Rev.* **2012**, *256*, 2453–2477.

(11) Claessens, C. G.; Hahn, U.; Torres, T. Phthalocyanines: From Outstanding Electronic Properties to Emerging Applications. *Chem. Rec.* **2008**, *8*, 75–97.

(12) Satake, A.; Kobuke, Y. Artificial Photosynthetic Systems: Assemblies of Slipped Cofacial Porphyrins and Phthalocyanines Showing Strong Electronic Coupling. *Org. Biomol. Chem.* **2007**, *5*, 1679–1691.

(13) Siebbeles, L. D. A.; Huijser, A.; Savenije, T. J. Effects of Molecular Organization on Exciton Diffusion in Thin Films of Bioinspired Light-Harvesting Molecules. *J. Mater. Chem.* **2009**, *19*, 6067–6072.

(14) Fassioli, F.; Dinshaw, R.; Arpin, P. C.; Scholes, G. D. Photosynthetic Light Harvesting: Excitons and Coherence. *J. R. Soc. Interface* **2014**, *11*, 20130901.

(15) Chenu, A.; Scholes, G. D. Coherence in Energy Transfer and Photosynthesis. *Annu. Rev. Phys. Chem.* **2015**, *66*, 69–96.

(16) Tant, J.; Geerts, Y. H.; Lehmann, M.; De Cupere, V.; Zucchi, G.; Laursen, B. W.; Bjørnholm, T.; Lemaur, V.; Marcq, V.; Burquel, A.; et al. Liquid Crystalline Metal-Free Phthalocyanines Designed for Charge and Exciton Transport. *J. Phys. Chem. B* **2005**, *109*, 20315–20323.

(17) Yoneya, M.; Miyamoto, A.; Shimizu, Y.; Fujii, A.; Ozaki, M. Origin of the High Carrier Mobilities of Nonperipheral Octahexyl Substituted Phthalocyanine. *J. Phys. Chem. C* **2015**, *119*, 23852–23858.

(18) da Silva Filho, D. A.; Coropceanu, V.; Gruhn, N. E.; de Oliveira Neto, P. H.; Brédas, J.-L. Intramolecular Reorganization Energy in Zinc Phthalocyanine and Its Fluorinated Derivatives: A Joint Experimental and Theoretical Study. *Chem. Commun. (Camb).* **2013**, *49*, 6069–6071.

(19) Huijser, A.; Savenije, T. J.; Meskers, S. C. J.; Vermeulen, M. J. W.; Siebbeles, L. D. A. The Mechanism of Long-Range Exciton Diffusion in a Nematically Organized Porphyrin Layer. *J. Am. Chem. Soc.* **2008**, *130*, 12496–12500.

(20) Gao, Y.; Chen, Y.; Li, R.; Bian, Y.; Li, X.; Jiang, J. Nonperipherally Octa(butyloxy)-Substituted Phthalocyanine Derivatives with Good Crystallinity: Effects of Metal-Ligand Coordination on the Molecular Structure, Internal Structure, and Dimensions of Self-Assembled Nanostructures. *Chem. - A Eur. J.* **2009**, *15*, 13241–13252.

(21) Rawat, N.; Pan, Z.; Manning, L. W.; Lamarche, C. J.; Cour, I.; Headrick, R. L.; Waterman, R.; Woll, A. R.; Furis, M. I. Macroscopic Molecular Ordering and Exciton Delocalization in Crystalline Phthalocyanine Thin Films. *J. Phys. Chem. Lett.* **2015**, *6*, 1834–1840.

(22) Aragó, J.; Troisi, A. Dynamics of the Excitonic Coupling in Organic Crystals. *Phys. Rev. Lett.* **2015**, *114*, 026402.

(23) Aragó, J.; Troisi, A. Regimes of Exciton Transport in Molecular Crystals in the Presence of Dynamic Disorder. *Adv. Funct. Mater.* **2015**, DOI:10.1002/adfm.201503888.

(24) Davydov, A. S. *Theory of Molecular Excitons*; Plenum: New York, 1971.

(25) Ortí, E.; Brédas, J. L.; Clarisse, C. Electronic Structure of Phthalocyanines: Theoretical Investigation of the Optical Properties of Phthalocyanine Monomers, Dimers, and Crystals. *J. Chem. Phys.* **1990**, *92*, 1228.

(26) Nakamura, H.; Truhlar, D. G. The Direct Calculation of Diabatic States Based on Configurational Uniformity. *J. Chem. Phys.* **2001**, *115*, 10353.

(27) Cave, R. J.; Newton, M. D. Multistate Treatments of the Electronic Coupling in Donor-Bridge-Acceptor Systems: Insights and Caveats from a Simple Model. *J. Phys. Chem. A* **2014**, *118*, 7221–7234.

(28) Rust, M.; Lappe, J.; Cave, R. J. Multistate Effects in Calculations of the Electronic Coupling Element for Electron Transfer Using the Generalized Mulliken−Hush Method. *J. Phys. Chem. A* **2002**, *106*, 3930–3940.

(29) Subotnik, J. E.; Yeganeh, S.; Cave, R. J.; Ratner, M. A. Constructing Diabatic States from Adiabatic States: Extending Generalized Mulliken-Hush to Multiple Charge Centers with Boys Localization. *J. Chem. Phys.* **2008**, *129*, 244101.

(30) Aragó, J.; Troisi, A. Excitonic Couplings between Molecular Crystal Pairs by a Multistate Approximation. *J. Chem. Phys.* **2015**, *142*, 164107.

(31) Scholes, G. D. Long-Range Resonance Energy Transfer in Molecular Systems. *Annu. Rev. Phys. Chem.* **2003**, *54*, 57–87.

(32) Hsu, C.-P.; You, Z.-Q.; Chen, H.-C. Characterization of the Short-Range Couplings in Excitation Energy Transfer. *J. Phys. Chem. C* **2008**, *112*, 1204–1212.

(33) Hestand, N. J.; Tempelaar, R.; Knoester, J.; Jansen, T. L. C.; Spano, F. C. Exciton Mobility Control through Sub-A Packing Modifications in Molecular Crystals. *Phys. Rev. B* **2015**, *91*, 195315.

(34) Renaud, N.; Grozema, F. C. Intermolecular Vibrational Modes Speed Up Singlet Fission in Perylenediimide Crystals. *J. Phys. Chem. Lett.* **2015**, *6*, 360–365.

(35) You, Z.-Q.; Hsu, C.-P. Theory and Calculation for the Electronic Coupling in Excitation Energy Transfer. *Int. J. Quantum Chem.* **2014**, *114*, 102–115.

(36) Hsu, C.-P. The Electronic Couplings in Electron Transfer and Excitation Energy Transfer. *Acc. Chem. Res.* **2009**, *42*, 509–518.

(37) Cave, R. J.; Newton, M. D. Generalization of the Mulliken-Hush Treatment for the Calculation of Electron Transfer Matrix Elements. *Chem. Phys. Lett.* **1996**, *249*, 15–19.

(38) Voityuk, A. A. Estimation of Electronic Coupling for Singlet Excitation Energy Transfer. *J. Phys. Chem. C* **2014**, *118*, 1478–1483.

(39) Voityuk, A. A. Fragment Transition Density Method to Calculate Electronic Coupling for Excitation Energy Transfer. *J. Chem. Phys.* **2014**, *140*, 244117.

(40) Hoyer, C. E.; Xu, X.; Ma, D.; Gagliardi, L.; Truhlar, D. G. Diabatization Based on the Dipole and Quadrupole: The DQ Method. *J. Chem. Phys.* **2014**, *141*, 114104.

(41) Kistler, K. A.; Spano, F. C.; Matsika, S. A Benchmark of Excitonic Couplings Derived from Atomic Transition Charges. *J. Phys. Chem. B* **2013**, *117*, 2032–2044.

(42) Ponder, J. W.; Richards, F. M. An Efficient Newton-like Method for Molecular Mechanics Energy Minimization of Large Molecules. *J. Comput. Chem.* **1987**, *8*, 1016–1024.

(43) Vydrov, O. a; Scuseria, G. E. Assessment of a Long-Range Corrected Hybrid Functional. *J. Chem. Phys.* **2006**, *125*, 234109.

(44) Francl, M. M.; Pietro, W. J.; Hehre, W. J.; Binkley, J. S.; Gordon, M. S.; DeFrees, D. J.; Pople, J. Self-Consistent Molecular Orbital Methods. XXIII. A Polarization-Type Basis Set for Second-Row Elements. *J. Chem. Phys.* **1982**, *77*, 3654.

(45) Rohrdanz, M. A.; Martins, K. M.; Herbert, J. M. A Long-Range-Corrected Density Functional That Performs Well for Both Ground-State Properties and Time-Dependent Density Functional Theory Excitation Energies, Including Charge-Transfer Excited States. *J. Chem. Phys.* **2009**, *130*, 054112.

(46) Malagoli, M.; Coropceanu, V.; da Silva Filho, D. A.; Brédas, J. L. A Multimode Analysis of the Gas-Phase Photoelectron Spectra in Oligoacenes. *J. Chem. Phys.* **2004**, *120*, 7490.

(47) Valiev, M.; Bylaska, E. J.; Govind, N.; Kowalski, K.; Straatsma, T. P.; Van Dam, H. J. J.; Wang, D.; Nieplocha, J.; Apra, E.; Windus, T. L.; et al. NWChem: A Comprehensive and Scalable Open-Source Solution for Large Scale Molecular Simulations. *Comput. Phys. Commun.* **2010**, *181*, 1477–1489.

(48) Troisi, A.; Orlandi, G. Dynamics of the Intermolecular Transfer Integral in Crystalline Organic Semiconductors. *J. Phys. Chem. A* **2006**, *110*, 4065–4070.

(49) Brédas, J.-L.; Beljonne, D.; Coropceanu, V.; Cornil, J. Charge-Transfer and Energy-Transfer Processes in Pi-Conjugated Oligomers and Polymers: A Molecular Picture. *Chem. Rev.* **2004**, *104*, 4971–5004.

(50) Van Mingroot, H.; De Backer, S.; van Stam, J.; Van der Auweraer, M.; De Schryver, F. C. The Emission at 669 Nm of Metal Free Phthalocyanine in Toluene and 1-Bromonaphthalene Solutions. *Chem. Phys. Lett.* **1996**, *253*, 397–402.

(51) Baeten, Y.; Fron, E.; Ruzié, C.; Geerts, Y. H.; Van Der Auweraer, M. Investigation of the Qx - Qy Equilibrium in a Metal-Free Phthalocyanine. *ChemPhysChem* **2015**, *16*, 3992–3996.

(52) Förster, T. 10th Spiers Memorial Lecture. Transfer Mechanisms of Electronic Excitation. *Discuss. Faraday Soc.* **1959**, *27*, 7–17.

(53) Marcus, R. A. Electron Transfer Reactions in Chemistry. Theory and Experiment. *Rev. Mod. Phys.* **1993**, *65*, 599–610.

(54) Barbara, P. F.; Meyer, T. J.; Ratner, M. A. Contemporary Issues in Electron Transfer Research. *J. Phys. Chem.* **1996**, *100*, 13148–13168.

(55) Fornari, R. P.; Aragó, J.; Troisi, A. A Very General Rate Expression for Charge Hopping in Semiconducting Polymers. *J. Chem. Phys.* **2015**, *142*, 184105.

(56) Elsaesser, T.; Kaiser, W. Vibrational and Vibronic Relaxation of Large Polyatomic Molecules in Liquids. *Annu. Rev. Phys. Chem.* **1991**, *42*, 83–107.

(57) Holstein, T. Studies of Polaron motion,Part I&II. *Ann. Phys. (N. Y).* **1959**, *8*, 325–389.

(58) McMahon, D. P.; Troisi, A. Evaluation of the External Reorganization Energy of Polyacenes. *J. Phys. Chem. Lett.* **2010**, *1*, 941–946.

(59) Martinelli, N. G.; Idé, J.; Sánchez-Carrera, R. S.; Coropceanu, V.; Brédas, J.-L.; Ducasse, L.; Castet, F.; Cornil, J.; Beljonne, D. Influence of Structural Dynamics on Polarization Energies in Anthracene Single Crystals. *J. Phys. Chem. C* **2010**, *114*, 20678–20685.

(60) Schröter, M.; Kühn, O. Interplay Between Nonadiabatic Dynamics and Frenkel Exciton Transfer in Molecular Aggregates: Formulation and Application to a Perylene Bismide Model. *J. Phys. Chem. A* **2013**, *117*, 7580–7588.

(61) Troisi, A.; Orlandi, G. Charge-Transport Regime of Crystalline Organic Semiconductors: Diffusion Limited by Thermal Off-Diagonal Electronic Disorder. *Phys. Rev. Lett.* **2006**, *96*, 086601.

(62) Fratini, S.; Mayou, D.; Ciuchi, S. The Transient Localization Scenario for Charge Transport in Crystalline Organic Materials. *Adv. Funct. Mater.* **2016**, 10.1002/adfm.201502386.

(63) Tully, J. C. Molecular Dynamics with Electronic Transitions. *J. Chem. Phys.* **1990**, *93*, 1061.

(64) Wang, L.; Akimov, A. V; Chen, L.; Prezhdo, O. V. Quantized Hamiltonian Dynamics Captures the Low-Temperature Regime of Charge Transport in Molecular Crystals. *J. Chem. Phys.* **2013**, *139*, 174109.

(65) Akimov, A. V; Long, R.; Prezhdo, O. V. Coherence Penalty Functional: A Simple Method for Adding Decoherence in Ehrenfest Dynamics. *J. Chem. Phys.* **2014**, *140*, 194107.

(66) Tempelaar, R.; Spano, F. C.; Knoester, J.; Jansen, T. L. C. Mapping the Evolution of Spatial Exciton Coherence through Time-Resolved Fluorescence. *J. Phys. Chem. Lett.* **2014**, *5*, 1505–1510.

(67) Wang, T.; Chan, W.-L. Dynamical Localization Limiting the Coherent Transport Range of Excitons in Organic Crystals. *J. Phys. Chem. Lett.* **2014**, *5*, 1812–1818.

(68) Valleau, S.; Saikin, S. K.; Yung, M.-H.; Aspuru Guzik, A. Exciton Transport in Thin-Film Cyanine Dye J-Aggregates. *J. Chem. Phys.* **2012**, *137*, 034109.

(69) Ke, Y.; Liu, Y.; Zhao, Y. Visualization of Hot Exciton Energy Relaxation from Coherent to Diffusive Regimes in Conjugated Polymers: A Theoretical Analysis. *J. Phys. Chem. Lett.* **2015**, *6*, 1741–1747.

(70) Kakade, S.; Ghosh, R.; Palit, D. K. Excited State Dynamics of Zinc–Phthalocyanine Nanoaggregates in Strong Hydrogen Bonding Solvents. *J. Phys. Chem. C* **2012**, *116*, 15155–15166.

(71) Mikhnenko, O.; Blom, P.; Nguyen, T.-Q. T. Exciton Diffusion in Organic Semiconductors. *Energy Environ. Sci.* **2015**, *8*, 1867–1888.

For Table of Contents use only

Exciton Dynamics in Phthalocyanine Molecular Crystals

Rocco P. Fornari, Juan Aragó,* Alessandro Troisi*